Original Article

Enhancing prognostic accuracy in invasive breast cancer by combining contrast-enhanced ultrasound and clinical data: a multicenter retrospective study

Shiyu Li[1,2], Yueming Li[1,2], Yongqi Fang[1], Zhiying Jin[1,2], Sisi Huang[1,2], Wei Wang[3], Kefah Mokbel[4], Yongjie Xu[5], Hua Yang[6], Zhili Wang[2]

[1]PLA Medical School, Beijing, China; [2]Department of Ultrasound, The First Medical Center of PLA General Hospital, Beijing, China; [3]Department of Ultrasound, The Fourth Medical Center of the PLA General Hospital, Beijing, China; [4]The London Breast Institute, Princess Grace Hospital, London, UK; [5]Department of Ultrasound, the Strategic Support Forces Specialty Medical Center, Beijing, China; [6]Outpatient Department, The First Medical Center of the PLA General Hospital, Beijing, China

Contributions: (I) Conception and design: S Li, Z Wang; (II) Administrative support: Z Wang; (III) Provision of study materials or patients: S Huang, W Wang, Y Xu, H Yang; (IV) Collection and assembly of data: S Li, Y Li, Z Jin; (V) Data analysis and interpretation: S Li, Y Fang, S Huang; (VI) Manuscript writing: All authors; (VII) Final approval of manuscript: All authors.

Correspondence to: Zhili Wang, PhD. Department of Ultrasound, The First Medical Center of PLA General Hospital, 28 Fuxing Road, Haidian District, Beijing 100853, China. Email: wzllg@sina.com; Hua Yang, PhD. Outpatient Department, The First Medical Center of the PLA General Hospital, 28 Fuxing Road, Haidian District, Beijing 100853, China. Email: 18600182799@163.com.

Background: Current predictive models for disease-free survival (DFS) in invasive breast cancer predominantly utilize clinical and pathological factors, with minimal incorporation of ultrasound (US) and contrast-enhanced ultrasound (CEUS) characteristics. This study aimed to establish a multimodal map integrating US, clinical features, and US data to enhance the prediction of DFS in invasive breast cancer.

Methods: The study utilized three retrospective datasets obtained from three academic medical centers, covering the period from March 2014 to December 2022. Clinical data, gray scale US, and CEUS were assessed in 942 adult patients undergoing breast cancer resection. The training and internal test sets were supplied by The First Medical Center of the PLA General Hospital, while the external test sets were sourced from The Fourth Medical Center of the PLA General Hospital and the Specialist Medical Center of the Strategic Support Forces. The patients were followed up by phone or clinic visits. DFS was evaluated as a prognostic outcome. Cox regression analysis identified prognostic factors, leading to the construction of three nomograms. The model performance was evaluated using the C-index, time-dependent receiver operating characteristic (ROC) curve, calibration, decision curve analysis (DCA), integrated discrimination improvement (IDI), and net reclassification index (NRI).

Results: A total of 942 patients were enrolled, with a mean age of 51.91 years [interquartile range (IQR), 44.25–58.69 years]. The patients were included with the median DFS of 36 months. Cox regression analysis identified menopausal status, body mass index (BMI), color Doppler flow imaging (CDFI), tumor size on CEUS, adjuvant/neoadjuvant chemotherapy, progesterone receptor (PR) status, and tumor-node-metastasis (TNM) staging as significant risk factors for invasive breast cancer. The nomogram combining US, CEUS, and clinical data demonstrated excellent predictive performance, achieving a C-index of 0.811 in the training set, 0.816 in the internal validation set, and 0.819 in the external validation set. Calibration curves confirmed that the predicted survival probabilities aligned closely with observed outcomes. Comparative analysis of ROC curves, IDI, NRI, and DCA confirmed that the integrated nomogram outperformed models based solely on US and clinical data or clinical data alone in predicting 24- and 36-month DFS.

Conclusions: The integration of CEUS and clinical factors for non-invasive DFS prediction improves personalized risk stratification, minimizing unnecessary interventions for low-risk patients and ensuring adequate monitoring for high-risk individuals. Additional prospective validation is required to establish its clinical applicability and incorporation into standard oncology practice.

Keywords: Breast cancer; contrast-enhanced ultrasound (CEUS); nomogram; prognosis

Submitted Jan 11, 2025. Accepted for publication Feb 16, 2025. Published online Feb 26, 2025.
doi: 10.21037/tcr-2025-96
View this article at: https://dx.doi.org/10.21037/tcr-2025-96

Introduction

Breast cancer is the most frequently encountered cancer globally and remains the second leading cause of cancer-related mortality among women, despite significant advancements in diagnostic techniques and therapeutic interventions (1,2). According to the National Cancer Research Center of Japan, two periods of heightened risk for recurrence following breast cancer surgery are identified, which are within the first to third years and the seventh to eighth years postoperatively. Research indicates that individuals with hormone receptor-positive breast cancer exhibit a significantly elevated risk of metastatic disease and recurrence within 8 to 10 years after surgery. Identifying individuals at high risk of recurrence and metastasis is essential for offering targeted preventive strategies and enabling early detection.

Clinical evidence has established that the presence of lymphovascular invasion in patients with breast cancer is linked to lymph node metastases and poor prognosis (3). Positive surgical resection margins have been associated with a higher risk of local recurrence in patients with early-stage breast cancer undergoing breast-conserving surgery (4,5). Various postoperative recurrence risk prediction models, including recurrence scores and 21-gene testing, have been created to identify patients at greater likelihood of breast cancer recurrence (6,7).

Numerous studies have shown that recurrence and metastasis significantly increase breast cancer-related mortality, highlighting a significant correlation between recurrence and survival outcomes (8,9). Early detection of recurrence and metastasis enhances curative treatment opportunities and improves survival rates (10). Thus, accurate identification of high-risk patients and vigilant postoperative surveillance are essential.

Multiple disease-free survival (DFS) prediction models have been created for breast cancer (11-13). The PREDICT model, which is widely used in the UK, achieved a C-index of 0.70–0.75, but its reliance on traditional clinical variables limits its generalizability (14); in addition, its predictive capability is constrained by its dependence on conventional clinical variables. The MammaPrint test, which includes gene expression profiles, demonstrated a higher area under the curve (AUC) (0.78–0.85) (15); however, its elevated cost and restricted accessibility hinder its broad clinical application. Studies have indicated that radiomics features gathered through magnetic resonance imaging (MRI) can effectively predict DFS in patients with invasive breast cancer. Radiomics nomograms have been demonstrated to estimate DFS with higher accuracy than that of traditional clinicopathological models {C-index [95% confidence interval (CI)]: 0.76 [0.74–0.77] *vs.* 0.72 [0.70–0.74]} (16). Additionally, contrast-enhanced ultrasound (CEUS), which assesses microvascular perfusion in lesions, offers supplementary information beyond conventional ultrasound (US) (17). Although CEUS has been increasingly utilized in breast cancer evaluation, its prognostic role in DFS prediction remains largely unexplored. Given the advantages of US and CEUS in real-time, non-invasive tumor characterization, integrating these imaging biomarkers with traditional clinicopathological factors may improve DFS prediction accuracy and clinical decision-making.

This multicenter, population-level, retrospective study aimed to develop two predictive models—one incorporating

Highlight box

Key findings

- The model incorporating ultrasound (US), contrast-enhanced ultrasound (CEUS), and clinical factors ($M_{US + CEUS + clinical}$ factors) demonstrated effective performance in predicting disease-free survival in patients with invasive breast cancer.

What is known and what is new?

- The combination of conventional US and clinical features can be used to predict disease-free survival in patients with breast cancer.
- The addition of CEUS to conventional US and clinical features provides a more robust model for predicting disease-free survival in patients with breast cancer.

What is the implication, and what should change now?

- Our findings suggest that the addition of blood flow visualization can improve the accuracy of predicting disease-free survival in patients with breast cancer.

US and clinical features alone and the other incorporating both US and CEUS—to predict DFS following invasive breast cancer surgery. The primary objectives were to identify patients at elevated risk for recurrence and metastasis and establish appropriate postoperative monitoring strategies for this population. We present this article in accordance with the TRIPOD reporting checklist (available at https://tcr.amegroups.com/article/view/10.21037/tcr-2025-96/rc).

Methods

Study design and population

This multicenter, retrospective cohort study was designed for the development and validation of a DFS prediction model (18). This study employed information from three hospitals: The First Medical Center of the PLA General Hospital, the Fourth Medical Center of The PLA General Hospital, and the Specialized Medical Center of the Strategic Support Forces. Our study focused on the development and validation of nomograms to predict outcomes after surgical resection of invasive breast cancer. A total of 5,427 patients who underwent mastectomy after US examination between March 2014 and December 2022 were included. Of these, 1,672 patients underwent CEUS prior to surgery after multidisciplinary consultation. In The First Medical Center of the PLA General Hospital, CEUS is a part of the standard assessment protocol for breast lesions before mastectomy, and the initial detection of a breast mass on conventional US is followed by CEUS evaluation.

In this study, patients were followed up at regular intervals: every 4 months during the initial 3 years, every 6–12 months for the fourth and fifth years, and annually thereafter. Follow-up assessments were conducted through office visits and telephone contact. The main endpoint of the study was DFS, defined as the duration from the initial pathological diagnosis to local tumor recurrence, distant metastasis, final monitoring, or death (7).

The dataset from The First Medical Center of the PLA General Hospital was divided into two cohorts: the development cohort (constituting approximately 70% of the data) and the internal validation cohort (constituting approximately 30% of the data). Datasets from The Fourth Medical Center of the PLA General Hospital, and the Specialized Medical Center of the Strategic Support Forces were used for external validation. To ensure comparability, the study followed strict inclusion and exclusion criteria. The exclusion criteria were as follows: patients who underwent US and/or CEUS after cancer diagnosis via US-guided core needle biopsy (18-gauge), vacuum-assisted breast biopsy, or excisional biopsy (n=121); unclear or improperly saved images that could not be fully assessed (n=73); metastatic disease or concurrent malignancy (n=56); positive surgical margins (n=41); missing human epidermal growth factor receptor 2 (HER-2) status (n=67); unknown tumor size (n=74); and loss to follow-up (n=298). Consequently, 942 standard-matched patients were included in the final analysis. All included patients had mass-like lesions identified on US, which were further evaluated by CEUS, leading to a final pathological diagnosis of unilateral invasive breast cancer. The study workflow is presented in *Figure 1*.

The study was conducted in accordance with the Declaration of Helsinki (as revised in 2013). This retrospective study received approval from the medical ethics committee of PLA General Hospital, China (No. S2024-749-01). All participating hospitals were informed and agreed with this study. The requirement for individual consent was waived due to the retrospective nature of the analysis.

Demographic and clinical characteristics

Demographic and clinical information were retrieved from patients' medical records. Clinical features included age, body mass index (BMI), history of benign breast disease, family history of breast cancer, menopausal status, age at menarche, and age at first labor.

Tumor characteristics were also collected, including tumor size, stage according to the 9th edition of the American Joint Committee on Cancer (AJCC) Cancer Staging Manual, histological grade, molecular subtype, pathological features, lymph node status, and treatment details (19).

US and CEUS image acquisition

All US and CEUS images were obtained using an Accuson S2000 system with high-frequency linear probes (6–15 MHz) (Siemens Healthineers, Erlangen, Germany). Lesions indicative of breast cancer were captured in both the horizontal and longitudinal planes, with color Doppler flow imaging (CDFI) providing additional information. In cases involving multiple lesions, analysis was restricted to the largest lesion. The lesion size as determined by the

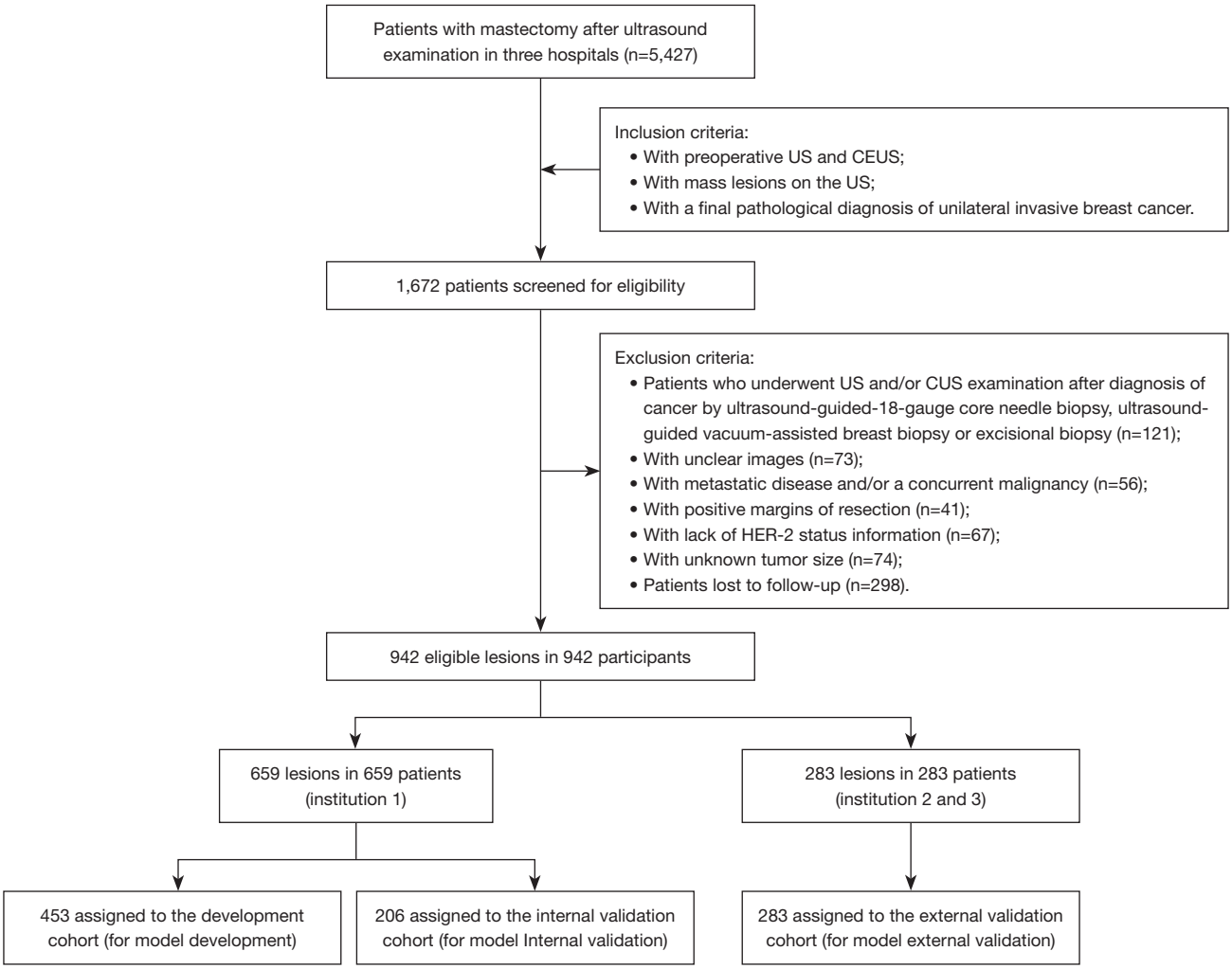

Figure 1 Study profile. Institution 1, The First Medical Center of the PLA General Hospital; institution 2, The Fourth Medical Center of the PLA General Hospital; institution 3, the Specialized Medical Center of the Strategic Support Forces. CEUS, contrast-enhanced ultrasound; US, ultrasound; HER-2, human epidermal growth factor receptor-2.

maximum diameter and as measured by US or CEUS was recorded and stored in a computer-based workstation. Sections with the largest lesion diameter or the richest CDFI signal, along with as much of the surrounding normal tissue as possible, were selected as the standard sections for CEUS evaluation. The mechanical index was set to 0.06–0.08, with SonoVue (Bracco, Milan, Italy) as the contrast agent. The contrast agent was administered into the anterior elbow vein at a rate of 5.0 mL/s and was followed by an infusion of 5.0–10.0 mL of normal saline. A minimum of 3 minutes of real-time images were recorded throughout the entire CEUS process, beginning at the time of injection.

US and CEUS feature evaluation

Image characteristics from the US and CEUS were extracted from the databases of the three participating medical institutions. Two experienced sonographers (Z.W. and S.L.), with 23 and 10 years of experience in breast US, respectively, evaluated these features blindly and independently. To evaluate the inter- and intraobserver uniformity, US images from 50 randomly chosen individuals were reassessed. Although both sonographers were aware that all patients had invasive breast cancer, they were blinded to the patients' DFS outcomes. Sonographer 2 (S.L.) repeated the procedure 2 weeks after the original protocol was implemented. The intraclass correlation coefficient

(ICC) was used to evaluate the inter- and intraobserver reliability of the multimodal US features, with features exhibiting an ICC >0.75 included in further analysis.

The US characteristics included shape (round/oval or irregular), margin (indistinct, spiculated, circumscribed, or microlobulated), echo pattern (hypoechoic, isoechoic, or heterotopic), orientation (parallel or nonparallel), posterior features (no posterior features, enhancement, shadowing, or combined pattern), high echo halo (absent or present), and calcification (absence, microcalcification, or coarse calcification). The blood flow signal on CDFI was graded from 0 to III according to the Adler method (20).

CEUS features were assessed using previously described methods (20). These included enhancement direction (central, centrifugal, or diffuse), enhanced intensity (hyperenhancement, isoenhancement, or hypo/nonenhancement), internal homogeneity (homogeneous or heterogeneous), size on CEUS (enlarged or not), perfusion defect (absent, fissure, or focal), enhancement shape (regular or irregular), enhancement margin (round or unbounded), radial or penetrating vessels (absent or present), wash-in time (earlier, concurrent, or later), and wash-out time (earlier, concurrent, or later). An enlarged size on CEUS was defined as a lesion 0.3 cm larger than that measured by US (20).

Statistical analyses

Statistical analyses were performed using SPSS 26 (IBM Corp., Armonk, NY, USA) and R software version 4.3.1 (The R Foundation for Statistical Computing, Vienna, Austria). The sample size was estimated based on DFS prediction performance. According to previous studies, an expected C-index improvement of 0.05–0.08 (from 0.72 to 0.78) was considered clinically relevant (11-13). A C-index improvement of 0.05–0.08 was considered clinically meaningful. Power analysis indicated that at least 900 patients were needed (α=0.05, β=0.10, power =90%). A total of 942 patients were included, ensuring statistical robustness for model development and validation. Continuous variables were expressed as the median with interquartile range (IQR), and comparisons between groups were conducted using the Mann-Whitney test. Categorical variables were expressed as frequencies and percentages, with comparisons made using the Chi-squared or Fisher exact test. Patients without survival outcome data were excluded from the final analysis. Univariate Cox regression analysis identified US, CEUS, and clinical characteristics as prognostic variables. The multivariate Cox regression analysis identified independent predictive markers for patients with invasive breast cancer via inclusion of the variables with a P value below 0.05. Nomograms were created from the independent prognostic variables. The Kaplan-Meier approach evaluated DFS and 95% confidence intervals (CIs), and the log-rank test determined the DFS differences between the training, internal validation, and external validation groups.

The Harrell concordance index (C-index) and 95% CIs were used to evaluate the predictive model's discrimination. The model's predictive power was further assessed using time-dependent receiver operating characteristic (ROC) curves and AUC. DeLong's test was used for AUC comparisons. Model validation was performed with k-fold cross-validation (k=10). To graphically compare projected and actual survival results, calibration curves were drawn from 1,000 bootstrapped samples.

Additionally, decision curve analysis (DCA), net reclassification index (NRI), and integrated discrimination improvement (IDI) were used to evaluate the nomogram's clinical value. These methods were also employed to examine if the US, CEUS, and clinical data model was more accurate than the US and clinical data model. X-tile software was used to determine the best nomogram cutoff value for total points, with patients being stratified into high- and low-risk categories. These groups' survival disparities throughout training, internal validation, and external validation cohorts were compared using Kaplan-Meier analysis and the log-rank test.

Results

DFS and clinical variables

A total of 942 breast cancer patients who underwent surgery and met the selection criteria were included in the analysis, with a mean age of 51.91 years (IQR, 44.25–58.69 years). The patients were included with the median DFS of 36 months. The demographic, US, and CEUS data for these patients are displayed in *Tables 1*,*2*. During follow-up, 156 patients (16.5%) experienced disease recurrence, with 69 (15.2%) patients in the internal training cohort, 36 (17.5%) in the internal validation cohort, and 51 (18.0%) in the external validation cohort. Among the 156 recurrence cases, 39 (25.0%) were local, 79 (50.6%) involved distant metastasis, 4 (2.5%) involved contralateral breast cancer, and 32 (20.5%) involved both local and distant recurrence. There were two breast cancer-related deaths (1.4%).

Table 1 Patient demographics and baseline characteristic in training and validation sets

Characteristics	Training set	Internal validation cohort		External validation cohort	
		Value	P value	Value	P value
Age (years)	51.94 [45, 59]	51.91 [44, 60]	0.98	50 [44, 57.75]	0.16
BMI (kg/m^2)	23.70 [21.6, 25.2]	24.21 [21.4, 26.4]	0.78	23.91 [21.26, 25.94]	0.41
Location			0.29		0.55
Subpapillary	6 (1.3)	8 (3.9)		8 (2.8)	
Upper outer quadrant	280 (61.8)	119 (57.8)		171 (60.4)	
Lower outer quadrant	64 (14.1)	32 (15.5)		34 (12.0)	
Upper inner quadrant	84 (18.5)	38 (18.4)		56 (19.8)	
Lower inner quadrant	19 (4.2)	9 (4.4)		14 (4.9)	
History of benign breast disease			0.59		0.55
Yes	103 (22.7)	43 (20.9)		59 (20.8)	
No	350 (77.3)	163 (79.1)		224 (79.2)	
Menopausal status			0.39		0.053
Yes	368 (81.2)	173 (84.0)		213 (75.3)	
No	85 (18.8)	33 (16.0)		70 (24.7)	
Menarche (years)			0.12		0.60
<12	30 (6.6)	10 (4.9)		14 (4.9)	
12–13	104 (23.0)	62 (30.1)		70 (24.7)	
≥14	319 (70.4)	134 (65.0)		199 (70.3)	
Time of first labor (years)			0.25*		0.11*
<20	7 (1.5)	2 (1.0)		4 (1.4)	
20–24	134 (29.6)	61 (29.6)		78 (27.6)	
25–29	264 (58.3)	122 (59.2)		164 (58.0)	
≥30	38 (8.4)	21 (10.2)		36 (12.7)	
Childless	10 (2.2)	0		1 (0.4)	
Family history of breast cancer			0.16		0.09
Yes	14 (3.1)	11 (5.3)		16 (5.7)	
No	439 (96.9)	195 (94.7)		267 (94.3)	
Size (cm)			0.77		0.83
<2	257 (56.7)	118 (57.3)		167 (59.0)	
2–5	175 (38.6)	76 (36.9)		103 (36.4)	
>5	21 (4.6)	12 (5.8)		13 (4.6)	
Multifocal/multicentric disease			0.44		0.27
Yes	65 (14.3)	25 (12.1)		23 (11.2)	
No	388 (85.7)	181 (87.9)		183 (88.8)	

Table 1 (*continued*)

Table 1 (*continued*)

Characteristics	Training set	Internal validation cohort		External validation cohort	
		Number	P value	Number	P value
Basal incisal margin invasion			0.68		0.08
Yes	16 (3.5)	6 (2.9)		18 (6.4)	
No	437 (96.5)	200 (97.1)		265 (93.6)	
Lympho-vascular invasion			0.95		0.81
Yes	58 (12.8)	26 (12.6)		38 (13.4)	
No	395 (87.2)	180 (87.4)		245 (86.6)	
Invasion of nerves			0.88		0.89
Yes	30 (6.6)	13 (6.3)		18 (6.4)	
No	423 (93.4)	193 (93.7)		265 (93.6)	
Skin or nipple invasion			0.09		0.06
Yes	22 (4.9)	17 (8.3)		24 (8.5)	
No	431 (95.1)	189 (91.7)		259 (91.5)	
ER			0.07		0.96
Negative	108 (23.8)	36 (17.5)		67 (23.7)	
Positive	345 (76.2)	170 (82.5)		216 (76.3)	
PR			0.03		0.93
Negative	325 (71.7)	164 (79.6)		202 (71.4)	
Positive	128 (28.3)	42 (20.4)		81 (28.6)	
HER-2			0.87		0.13
Negative	151 (33.3)	70 (34.0)		173 (61.1)	
Positive	302 (66.7)	136 (66.0)		110 (38.9)	
Ki-67			0.16		0.37
Negative	82 (18.1)	47 (22.8)		44 (15.5)	
Positive	371 (81.9)	159 (77.2)		239 (84.5)	
Molecular typing			0.41		0.18
Luminal A	160 (35.3)	73 (35.4)		118 (41.7)	
Luminal B	94 (20.8)	51 (24.8)		53 (18.7)	
HER2-enriched	150 (33.1)	67 (32.5)		92 (32.5)	
Triple-negative	49 (10.8)	15 (7.3)		20 (7.1)	
Lymph node			0.71		0.70
Yes	185 (40.8)	81 (39.3)		163 (57.6)	
No	268 (59.2)	125 (60.7)		120 (42.4)	

Table 1 (*continued*)

Table 1 (*continued*)

Characteristics	Training set	Internal validation cohort		External validation cohort	
		Number	P value	Number	P value
TNM			0.55*		0.52*
0	2 (0.4)	1 (0.5)		0	
I	198 (43.7)	77 (37.4)		110 (38.9)	
II	165 (36.4)	88 (42.7)		116 (41.0)	
III	74 (16.3)	35 (17.0)		48 (17.0)	
IV	14 (3.1)	5 (2.4)		9 (3.2)	
Surgery			0.81		0.08
Modified radical mastectomy	279 (61.6)	130 (63.1)		172 (60.8)	
Radical mastectomy	106 (23.4)	49 (23.8)		82 (29.0)	
Breast conservation surgery	68 (15.0)	27 (13.1)		29 (10.2)	
Adjuvant neoadjuvant chemotherapy			0.97		0.13
Yes	40 (8.8)	18 (8.7)		35 (12.4)	
No	413 (91.2)	188 (91.3)		248 (87.6)	
Adjuvant chemotherapy			0.20		0.71
Yes	361 (79.7)	155 (75.2)		222 (78.4)	
No	92 (20.3)	51 (24.8)		61 (21.6)	
Adjuvant radiation			0.57		0.34
Yes	120 (26.5)	59 (28.6)		66 (23.3)	
No	333 (73.5)	147 (71.4)		217 (76.7)	
Adjuvant targeted therapy			0.67		0.05
Yes	101 (22.3)	49 (23.8)		81 (28.6)	
No	352 (77.7)	157 (76.2)		202 (71.4)	
Adjuvant endocrine therapy			0.96		0.14
Yes	300 (66.2)	136 (66.0)		202 (71.4)	
No	153 (33.8)	70 (34.0)		81 (28.6)	

Data are expressed as median [interquartile range] or n (%). *, Fisher exact test. BMI, body mass index; ER, estrogen receptor; PR, progesterone receptor; HER-2, human epidermal growth factor receptor-2; TNM, tumor node metastasis.

Screening indicators with DFS predictive ability

In the training cohort, several factors demonstrated statistically significant associations with prognosis, including BMI (P=0.002), menopausal status (P=0.048), CDFI (P=0.004), lesion size on CEUS (P<0.001), adjuvant/neoadjuvant chemotherapy (P<0.001), progesterone receptor (PR) status (P=0.001), tumor-node-metastasis (TNM) staging (P<0.001), and lympho-vascular invasion (P<0.001).

Multivariate Cox regression analysis, comprising US, CEUS, and clinical factors, identified the following as independent risk factors for poor prognosis: BMI (P=0.10), CDFI (P=0.10), CEUS lesion size (P<0.001), menopausal status (P=0.09), adjuvant/neoadjuvant chemotherapy (P=0.02), PR status (P=0.002), TNM staging (P<0.001), and lymphovascular invasion (P<0.001) (*Figures 2*,*3*, *Table 3*).

Table 2 Patient ultrasound, contrast-enhanced and ultrasound characteristic in training and validation sets

Characteristics	Training set	Internal validation cohort		External validation cohort	
		Number	P value	Number	P value
Shape			0.45		0.81
Irregular	440 (97.1)	198 (96.1)		274 (96.8)	
Round/oval	13 (2.9)	8 (3.9)		9 (3.2)	
Margin			0.45		0.70
Indistinct	145 (32.0)	63 (30.6)		102 (36.0)	
Spiculated	220 (48.5)	110 (53.4)		131 (46.3)	
Circumscribed	36 (7.9)	16 (7.8)		22 (7.8)	
Microlobulated	52 (11.5)	17 (8.3)		28 (9.9)	
Echo pattern			0.26		0.14
Hypoechoic	411 (90.7)	181 (87.9)		247 (87.3)	
Isoechoic or heterotopic	67 (10.2)	25 (12.1)		36 (12.7)	
Orientation			0.93		0.36
Parallel	227 (50.1)	104 (50.5)		132 (46.6)	
Not parallel	226 (49.9)	102 (49.5)		151 (53.4)	
Posterior features			0.21		0.65
No posterior features	320 (70.6)	138 (67.0)		204 (72.1)	
Enhancement	37 (8.2)	11 (5.3)		54 (19.1)	
Shadowing	80 (17.7)	46 (22.3)		18 (6.4)	
Combined pattern	16 (3.5)	11 (5.3)		7 (2.5)	
High echo halo			0.21		0.34
Absent	153 (33.8)	80 (38.8)		106 (37.5)	
Present	300 (66.2)	126 (61.2)		177 (62.5)	
Calcification			0.14		0.73
Absent	277 (61.1)	124 (60.2)		179 (63.3)	
Microcalcification	159 (35.1)	67 (32.5)		96 (33.9)	
Coarse calcification	17 (3.8)	15 (7.3)		8 (2.8)	
CDFI			0.91		0.14
0	95 (21.0)	48 (23.3)		63 (22.3)	
I	82 (18.1)	38 (18.4)		42 (14.8)	
II	134 (29.6)	59 (28.6)		69 (24.4)	
III	142 (31.3)	61 (29.6)		109 (38.5)	
Enhancement direction			0.34		0.81
Central	305 (67.3)	138 (67.0)		192 (67.8)	
Centrifugal	48 (10.6)	29 (14.1)		26 (9.2)	
Diffuse	100 (22.1)	39 (18.9)		65 (23.0)	

Table 2 (*continued*)

Table 2 (*continued*)

Characteristics	Training set	Internal validation cohort		External validation cohort	
		Number	P value	Number	P value
Enhanced intensity			0.42		0.39
Hyper-enhancement	404 (89.2)	184 (89.3)		261 (92.2)	
Iso-enhancement	19 (4.2)	5 (2.4)		8 (2.8)	
Hypo/non-enhancement	30 (6.6)	17 (8.3)		14 (4.9)	
Internal homogeneity			0.72		0.44
Homogeneous	72 (15.9)	35 (17.0)		39 (13.8)	
Heterogeneous	381 (84.1)	171 (83.0)		244 (86.2)	
Size on CEUS			0.08		0.20
Enlarged	298 (65.8)	121 (58.7)		173 (61.1)	
Not enlarged	155 (34.2)	85 (41.3)		110 (38.9)	
Perfusion defect			0.25		0.44
Absent	272 (60.0)	121 (58.7)		175 (61.6)	
Fissure	36 (7.9)	10 (4.9)		28 (9.9)	
Focal	145 (32.0)	75 (36.4)		80 (28.3)	
Enhancement shape			0.32		0.22
Regular	80 (17.7)	30 (14.6)		40 (14.1)	
Irregular	373 (82.3)	176 (85.4)		243 (85.9)	
Enhancement margin			0.56		0.60
Round	106 (23.4)	44 (21.4)		71 (25.1)	
Unboundary	347 (76.6)	162 (78.6)		212 (74.9)	
Radial or penetrating vessels			0.90		0.29
Absent	240 (53.0)	108 (52.4)		138 (48.8)	
Present	213 (47.0)	98 (47.6)		145 (51.2)	
Wash-in time			0.62		0.07
Earlier	20 (4.4)	6 (2.9)		269 (95.1)	
Meantime	23 (5.1)	12 (5.8)		5 (1.8)	
Later	410 (90.5)	188 (91.3)		9 (3.2)	
Wash-out time			0.64		0.28
Earlier	20 (4.4)	7 (3.4)		14 (4.9)	
Meantime	30 (6.6)	17 (8.3)		11 (3.9)	
Later	403 (89.0)	182 (88.3)		258 (91.2)	

Data are expressed as n (%). CDFI, color Doppler flow imaging; CEUS, contrast-enhanced ultrasound.

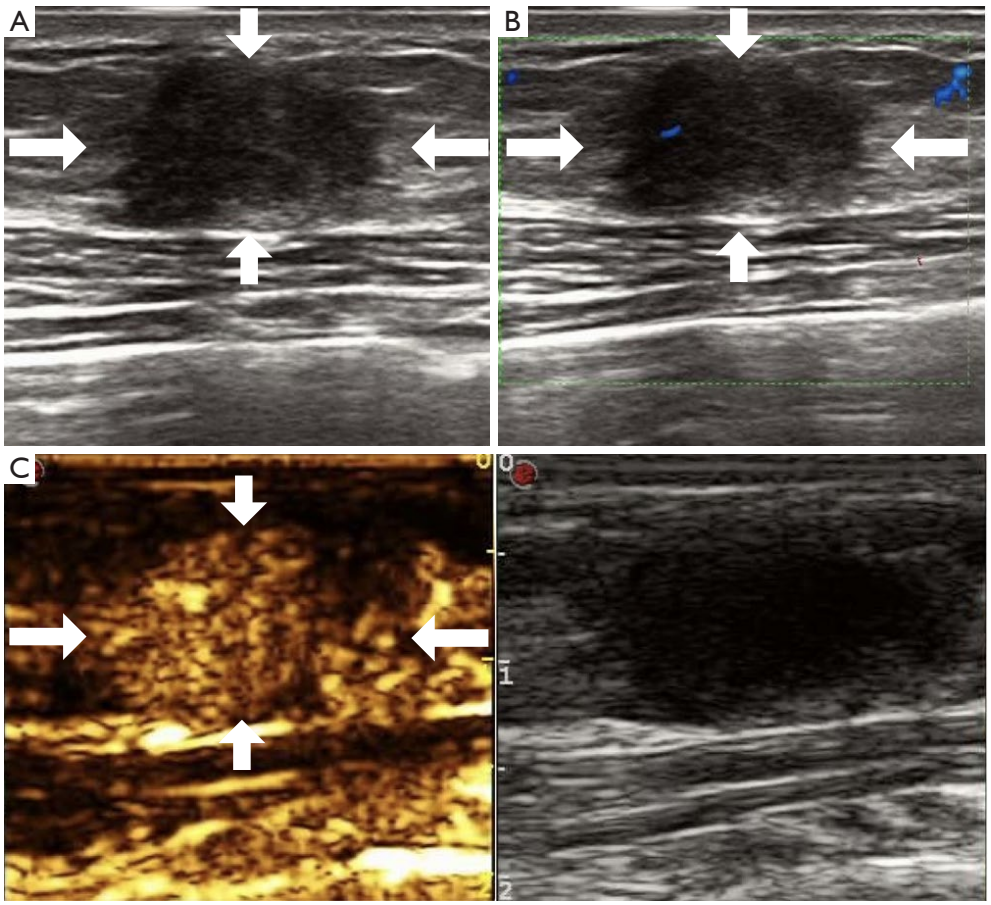

Figure 2 A 43-year-old woman with breast cancer on the left side. (A) B-mode ultrasound image showed irregular echoic lesions in the mammary gland with unclear boundaries (white arrows). (B) Color Doppler flow imaging showed grade I blood flow distribution* (white arrows); (C) CEUS showed an unseen enlargement of the lesion (white arrows). *, according to Adler blood flow grading results. CEUS, contrast-enhanced ultrasound.

A separate multivariate Cox regression analysis for US and clinical factors indicated that BMI (P=0.04), CDFI (P=0.10), menopausal status (P=0.10), adjuvant/neoadjuvant chemotherapy (P=0.008), PR status (P=0.004), TNM staging (P=0.06), and lympho-vascular invasion (P<0.001) served to be distinct indicators of poor prognosis (*Table 4*).

Finally, a multivariate Cox regression analysis of only clinical factors showed that BMI (P=0.04), menopausal status (P=0.07), adjuvant/neoadjuvant chemotherapy (P=0.003), PR status (P=0.004), TNM staging (P=0.03), and lympho-vascular invasion (P<0.001) were the independent risk variables for poor prognosis (*Table 5*).

Nomograms for invasive breast cancer prognosis

Nomograms were created using the individual prognostic variables identified from the analyses, including the nomogram model based on US, CEUS, and clinical characteristics ($M_{US+CEUS+clinical}$), nomogram model based on US and clinical characteristics ($M_{US+clinical}$), and nomogram model based on clinical characteristics ($M_{clinical}$) to predict DFS at 24, 36, and 60 months (*Figure 4*). The nomograms' performance was evaluated, resulting in a C-index of 0.811 (95% CI: 0.768–0.854) for $M_{US+CEUS+clinical}$, 0.794 (95% CI: 0.751–0.837) for $M_{US+clinical}$, and 0.788 (95% CI: 0.745–0.831) for $M_{clinical}$ in the training cohort; the validation cohorts

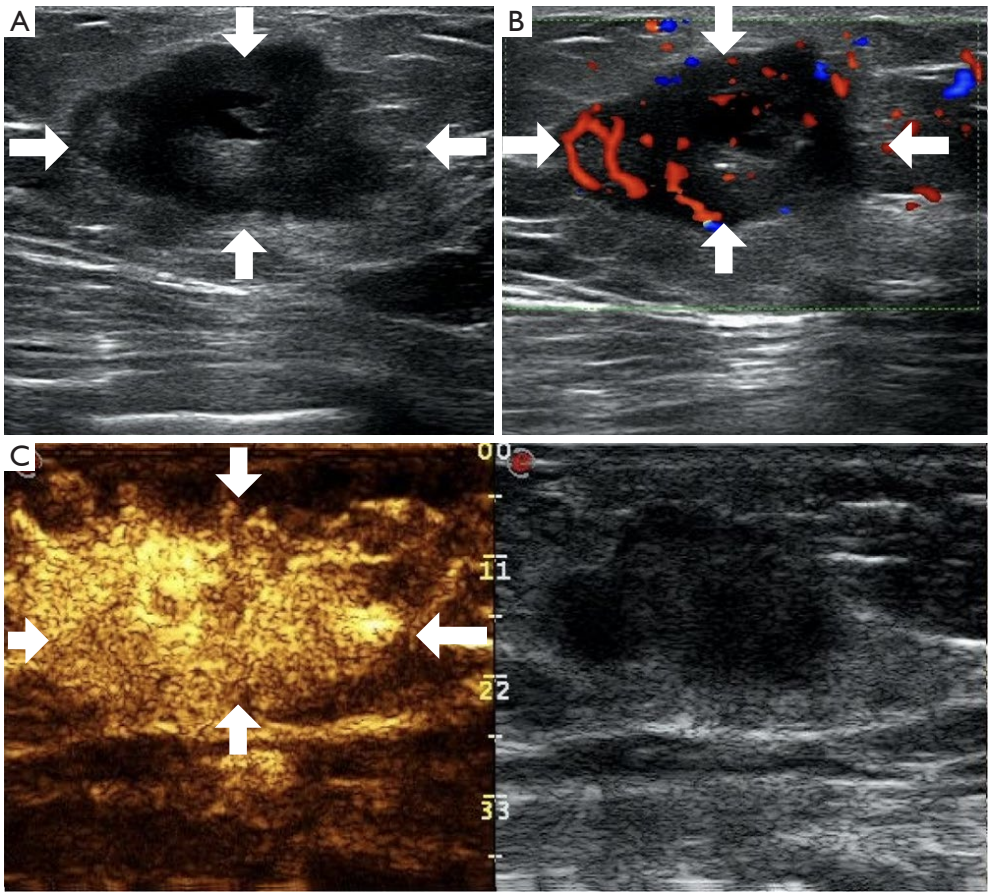

Figure 3 A 51-year-old woman with breast cancer on the right side. (A) B-mode ultrasound image showed irregular hypoechoic lesions (white arrows) with unclear boundaries. (B) Color Doppler flow imaging showed a grade III flow distribution* (white arrows). (C) CEUS showed high enhancement, irregular shape, and increased volume on CEUS, accompanied by penetrating vessels (white arrows). *, according to Adler blood flow grading results. CEUS, contrast-enhanced ultrasound.

Table 3 Univariate and multivariate Cox proportional hazards regression analysis based on ultrasound, CEUS and clinical data in the training set

Variables	Univariate analysis		Multivariate analysis	
	HR (95% CI)	P value	HR (95% CI)	P value
BMI	1.12 (1.04–1.21)	0.002*	1.07 (0.99–1.16)	0.10
CDFI	1.38 (1.11–1.73)	0.004*	1.21 (0.96–1.53)	0.10
Size on CEUS	3.96 (1.96–7.97)	<0.001*	1.48 (0.37–4.38)	<0.001*
Menopausal status	2.20 (1.01–4.81)	0.048*	1.98 (0.90–4.36)	0.09
Adjuvant neoadjuvant chemotherapy	3.49 (1.93–6.29)	<0.001*	2.06 (1.11–3.84)	0.02*
PR	0.45 (0.28–0.73)	0.001*	0.46 (0.28–0.75)	0.002*
TNM	2.07 (1.57–2.72)	<0.001*	5.33 (3.02–9.42)	<0.001*
Lympho-vascular invasion	6.15 (3.64–10.01)	<0.001*	7.63 (3.51–16.6)	<0.001*

*, statistical significance. CEUS, contrast-enhanced ultrasound; HR, hazard ratio; CI, confidence interval; BMI, body mass index; CDFI, color Doppler flow imaging; PR, progesterone receptor; TNM, tumor-node-metastasis.

Table 4 Univariate and multivariate Cox proportional hazards regression analysis based on ultrasound and clinical data in the training set

Variables	Univariate analysis		Multivariate analysis	
	HR (95% CI)	P value	HR (95% CI)	P value
BMI	1.12 (1.04–1.21)	0.002*	1.09 (1.00–1.18)	0.04*
CDFI	1.38 (1.11–1.73)	0.004*	1.22 (0.97–1.53)	0.10
Menopausal status	2.20 (1.01–4.81)	0.048*	1.91 (0.87–4.21)	0.10
Adjuvant neoadjuvant chemotherapy	3.49 (1.93–6.29)	<0.001*	2.31 (1.25–4.27)	0.008*
PR	0.45 (0.28–0.73)	0.001*	0.49 (0.30–0.80)	0.004*
TNM	2.07 (1.57–2.72)	<0.001*	1.34 (0.99–1.83)	0.06
Lympho-vascular invasion	6.15 (3.64–10.01)	<0.001*	4.41 (2.56–7.61)	<0.001*

*, statistical significance. HR, hazard ratio; CI, confidence interval; BMI, body mass index; CDFI, color Doppler flow imaging; PR, progesterone receptor; TNM, tumor-node-metastasis.

Table 5 Univariate and multivariate Cox proportional hazards regression analysis based on clinical data in the training set

Variables	Univariate analysis		Multivariate analysis	
	HR (95% CI)	P value	HR (95% CI)	P value
BMI	1.12 (1.04–1.21)	0.002*	1.09 (1.00–1.18)	0.04*
Menopausal status	2.20 (1.01–4.81)	0.048*	2.05 (0.93–4.5)	0.07
Adjuvant neoadjuvant chemotherapy	3.49 (1.93–6.29)	<0.001*	2.52 (1.37–4.63)	0.003*
PR	0.45 (0.28–0.73)	0.001*	0.49 (0.30–0.79)	0.004*
TNM	2.07 (1.57–2.72)	<0.001*	1.41 (1.04–1.91)	0.03*
Lympho-vascular invasion	6.15 (3.64–10.01)	<0.001*	4.43 (2.58–7.63)	<0.001*

*, statistical significance. HR, hazard ratio; CI, confidence interval; BMI, body mass index; PR, progesterone receptor; TNM, tumor-node-metastasis.

exhibited similar results, with C-indices of 0.816 (95% CI: 0.764–0.869), 0.799 (95% CI: 0.746–0.852), and 0.786 (95% CI: 0.733–0.839) in the internal validation cohort and C-indices of 0.819 (95% CI: 0.766–0.872), 0.743 (95% CI: 0.690–0.796), and 0.719 (95% CI: 0.666–0.772) in the external validation cohort, respectively.

K-fold cross-validation (k=10) indicated high AUC values for all models at 24, 36, and 60 months in both the training and validation sets, demonstrating robust discriminatory ability (*Figure 5* and *Table 6*).

Comparison of the three nomograms

DCA indicated that $M_{US+CEUS+clinical}$ provided superior net benefits and a broader range of threshold probabilities compared to $M_{US+clinical}$ and $M_{clinical}$ in both the training and validation cohorts (*Figure 6*). Calibration curves for all three models showed the strong agreement between predicted and observed outcomes (*Figures 7-9*).

NRI and IDI analyses also demonstrated that $M_{US+CEUS+clinical}$ outperformed the other models in predicting DFS at 24 and 36 months across all cohorts (*Tables 7,8*). At 60 months, $M_{US+CEUS+clinical}$ showed superior performance only in the training set, while the remaining models did not demonstrate significant variations at any of the three time points (*Table 9*).

Ability of the nomograms to assess patient risk

The total scores for each patient were computed using the nomograms, and X-tile software was employed to ascertain the best cutoff values for risk stratification. Patients were categorized into low- and high-risk groups for each model according to the follow cutoffs: $M_{US+CEUS+clinical}$, 121.90,

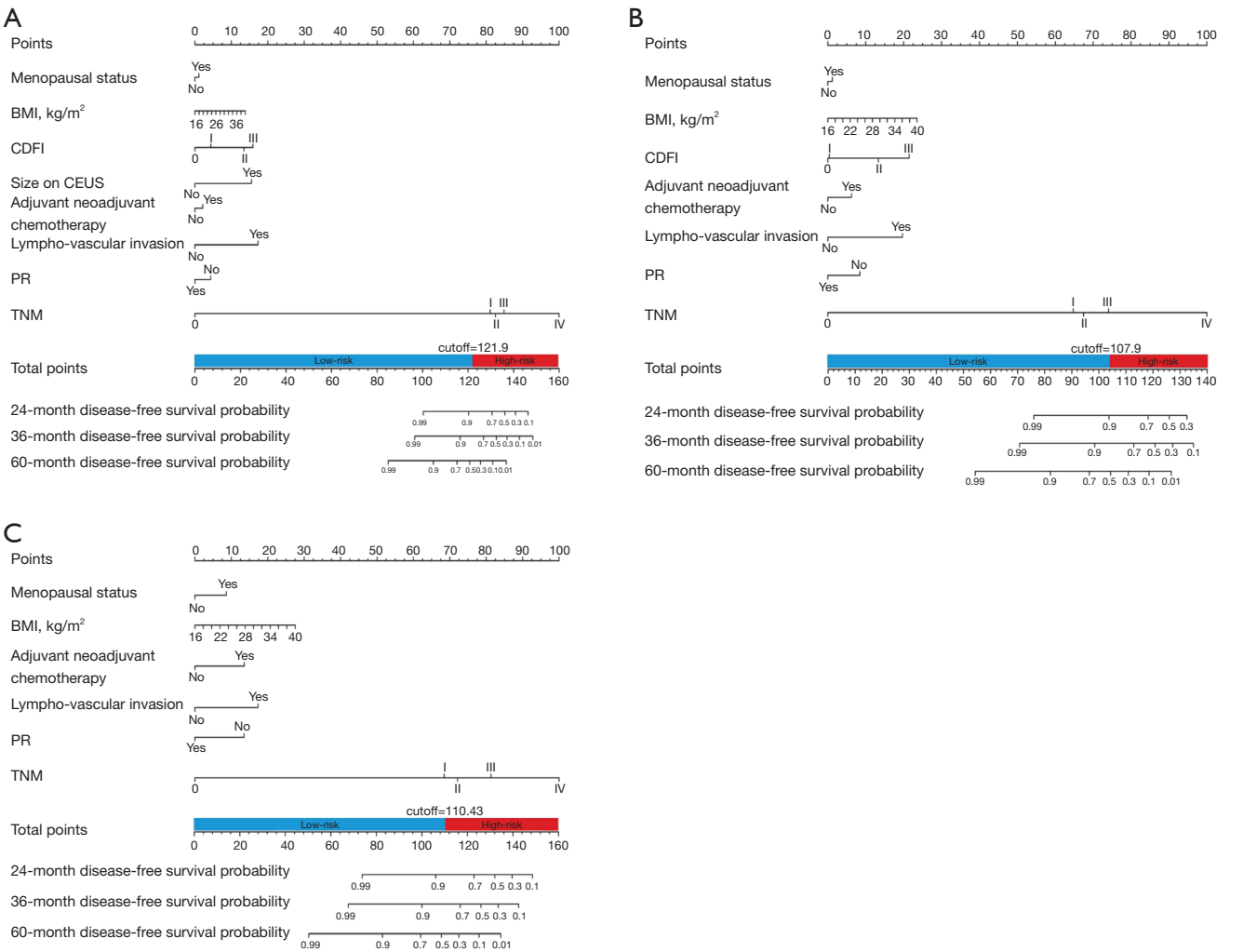

Figure 4 Nomograms of (A) $M_{US+CEUS+clinical}$, (B) $M_{US+clinical}$, and (C) $M_{clinical}$ for DFS at 24, 36, and 60 months. The presence or absence of each clinical feature indicates a certain number of points. The number of points for each clinical feature is in the first row. The presence of features is associated with the number of points generated using the nomograms. The "rms" package in R was used to analyze the results of Cox analysis. The scores for each feature are added together to generate an overall score. The total scores correspond to probabilities of disease-free survival at 24, 36, and 60 months, respectively. $M_{US+CEUS+clinical}$, nomogram model based on US, CEUS, and clinical characteristics; $M_{US+clinical}$, nomogram model based on US and clinical characteristics; $M_{clinical}$, nomogram model based on clinical characteristics; BMI, body mass index; CDFI, color Doppler flow imaging; CEUS, contrast-enhanced ultrasound; PR, progesterone receptor; TNM, tumor node metastasis; DFS, disease-free survival; US, ultrasound.

$M_{US+clinical}$, cutoff 107.90; and $M_{clinical}$, cutoff 110.43. Kaplan-Meier survival analysis with the log-rank test revealed significant disparities in DFS between the low- and high-risk groups in all models and across all datasets (all P values <0.0001; *Figure 10*). Higher risk scores were consistently associated with worse outcomes across all models.

Discussion

Our study developed nomograms to predict DFS in patients with invasive breast cancer by integrating clinical, pathological, and imaging features derived from conventional US and CEUS. These models—$M_{US+CEUS+clinical}$,

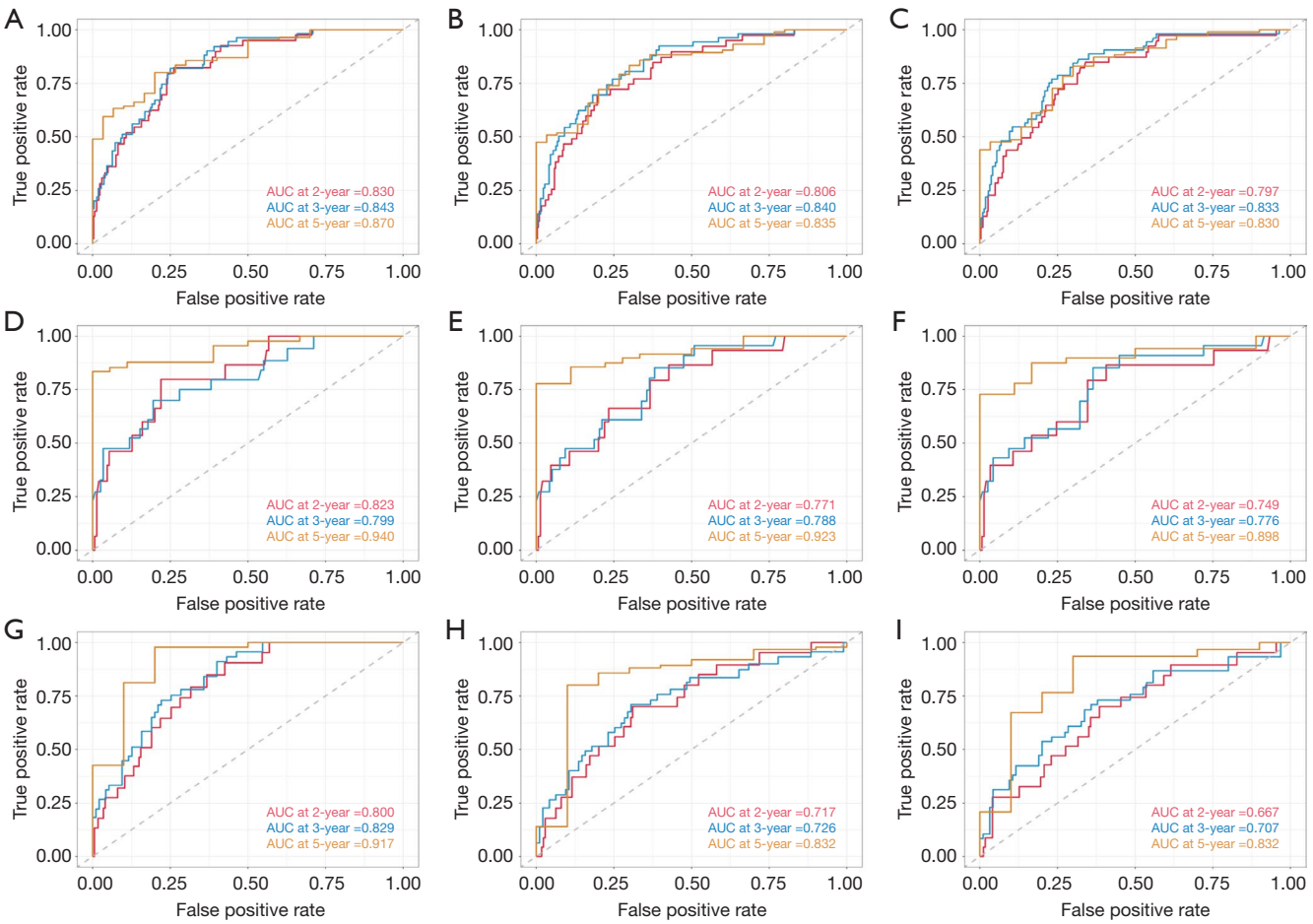

Figure 5 The ROC curves of $M_{US+CEUS+clinical}$, $M_{US+clinical}$, and $M_{clinical}$ in the (A-C) training cohort, (D-F) internal test cohort, and (G-I) external validation cohort were determined and compared. $M_{US+CEUS+clinical}$, nomogram model based on US, CEUS, and clinical characteristics; $M_{US+clinical}$, nomogram model based on US and clinical characteristics; $M_{clinical}$, nomogram model based on clinical characteristics; AUC, area under the curve; ROC, receiver operating characteristic; CEUS, contrast-enhanced ultrasound; US, ultrasound.

Table 6 AUC comparison of $M_{US+CEUS+clinical}$, $M_{US+clinical}$, and $M_{clinical}$ models in training, internal validation, and external validation sets

Model	Training set			Internal validation cohort			External validation cohort		
	24-month	36-month	60-month	24-month	36-month	60-month	24-month	36-month	60-month
$M_{US+CEUS+clinical}$	0.830	0.843	0.870	0.823	0.799	0.940	0.800	0.829	0.917
$M_{US+clinical}$	0.806	0.840	0.835	0.771	0.788	0.923	0.717	0.726	0.832
$M_{clinical}$	0.797	0.833	0.830	0.749	0.776	0.898	0.677	0.707	0.832

AUC, area under the curve; $M_{US+CEUS+clinical}$, nomogram model based on US, CEUS, and clinical characteristics; $M_{US+clinical}$, nomogram model based on US and clinical characteristics; $M_{clinical}$, nomogram model based on clinical characteristics; US, ultrasound; CEUS, contrast-enhanced ultrasound.

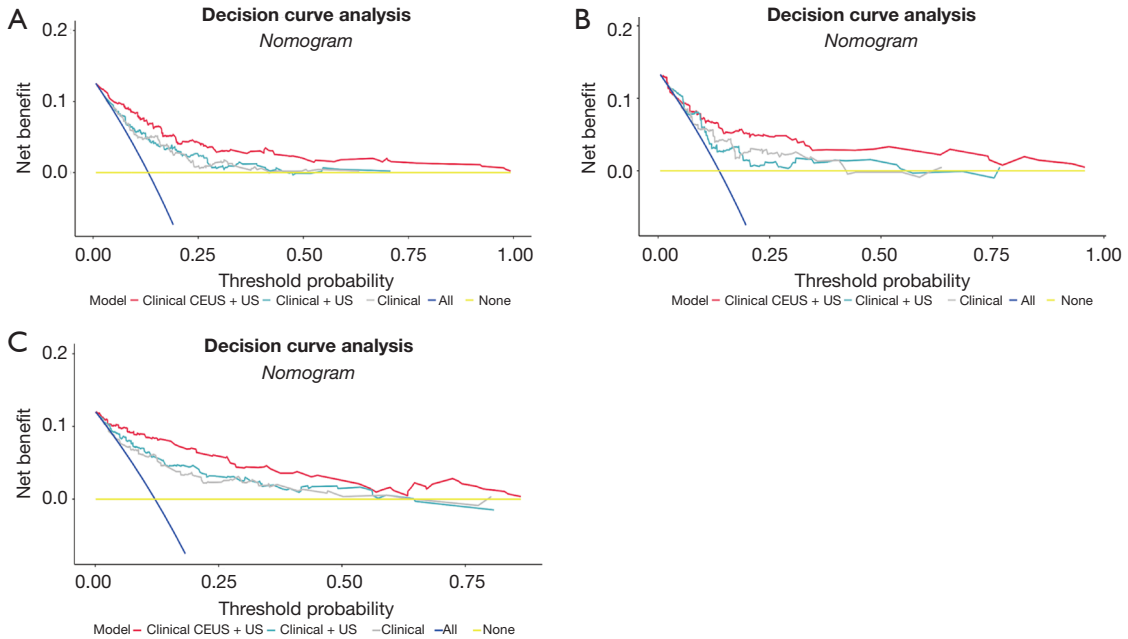

Figure 6 The DCA of predicted DFS for the (A) training group, (B) internal validation group, (C) and external validation group. CEUS, contrast-enhanced ultrasound; US, ultrasound; DCA, decision curve analysis; DFS, disease-free survival.

$M_{US+clinical}$, and $M_{clinical}$—aimed to provide a comprehensive assessment of individual risk for adverse outcomes in this patient population. The comparison of predictive power across the three models demonstrated that the $M_{US+CEUS+clinical}$ model had superior performance in predicting DFS compared to $M_{US+clinical}$ and $M_{clinical}$ in the training, internal validation, and external validation cohorts.

In the $M_{US+CEUS+clinical}$ nomogram, multivariate Cox regression analysis identified BMI (P=0.10), CDFI (P=0.10), size on CEUS (P<0.001), menopausal status (P=0.09), adjuvant/neoadjuvant chemotherapy (P=0.02), PR status (P=0.002), TNM classification (P<0.001), and lymphatic vascular invasion (P<0.001) as independent risk factors for DFS. Our findings align with previous studies indicating that menopausal status, PR status, and TNM classification significantly impact breast cancer prognosis (21-24).

Lymphatic vascular invasion, in particular, emerged as a crucial factor influencing DFS. It represents a critical early event in the metastatic process, in which tumor cells invade lymphatic and blood vessels (25), facilitating metastasis and negatively impacting the prognosis of breast cancer (26,27). Although the role of lymphatic invasion in breast cancer prognosis has been recognized, studies with long-term follow-up in well-characterized patient cohorts remain limited.

Although previous research has explored the predictive value of CDFI and CEUS in identifying breast lesions and lymph node metastasis, their role in predicting DFS in invasive breast cancer has not been fully examined (28). Our study, however, identified CDFI and tumor size on CEUS as significant predictors of DFS. This is consistent with existing literature, which suggests that enhanced vasculature and a balanced distribution of tumor blood vessels are associated with better predictive outcomes compared to conventional US imaging (29). Early identification of poor prognosis using CDFI and CEUS may allow for timely clinical interventions, significantly improving patients' life quality and chances of survival.

In this study, the predictive ability of the $M_{US+CEUS+clinical}$ model for breast cancer recurrence and metastasis was superior to that of the $M_{US+clinical}$ and $M_{clinical}$ models. Tumor progression relies on angiogenesis, necessitating additional vasculature beyond the oxygen diffusion limit (30). A variety of noninvasive imaging techniques, such as color Doppler, power Doppler, CEUS, computed tomography (CT), and MRI, have been employed to identify alterations in neovascularization associated with malignancy. Nonetheless, CDFI is limited in its ability to identify blood vessels that are larger than 100–200 μm (17).

Yu *et al.* (31) demonstrated that a US-based radiomics

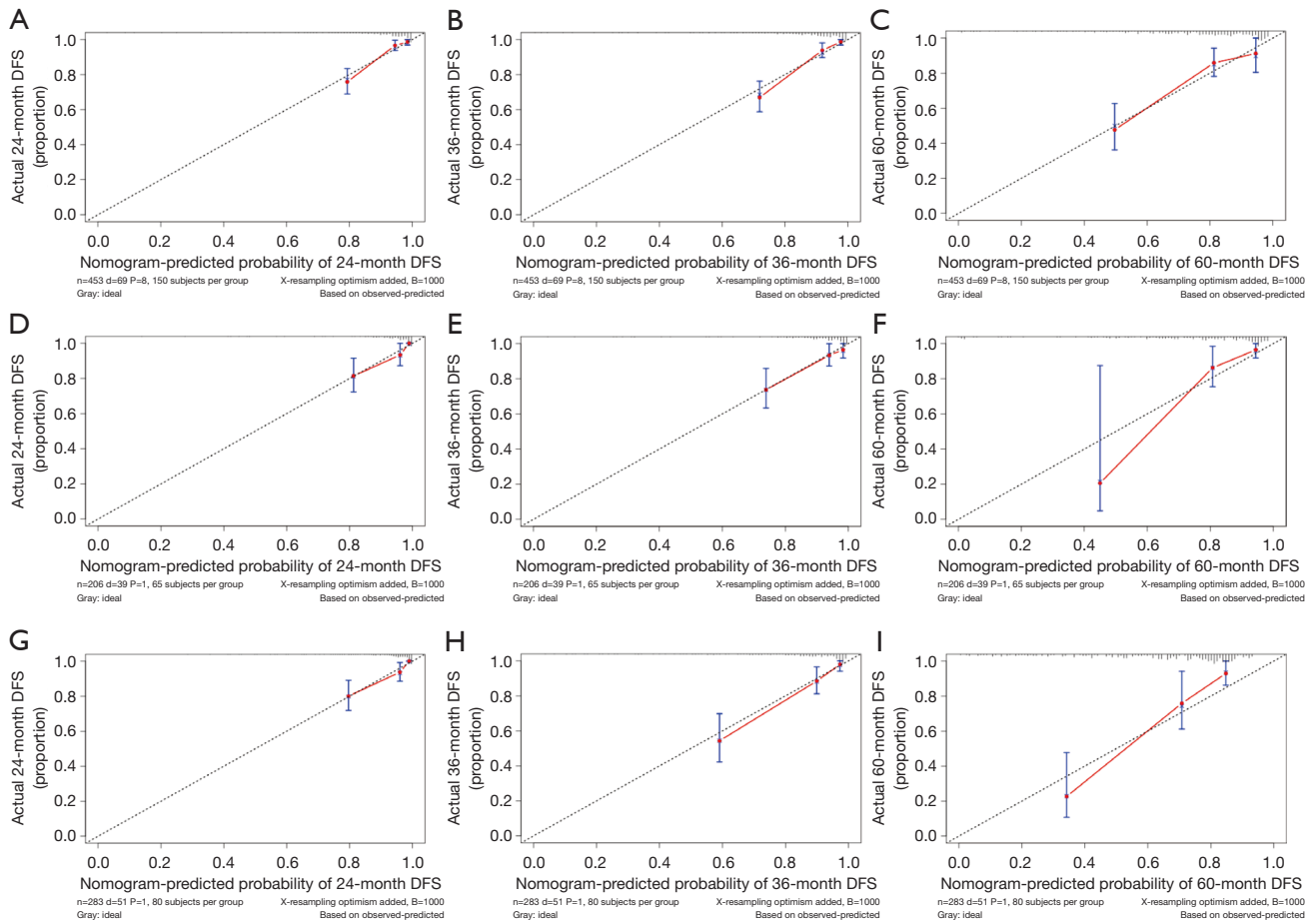

Figure 7 Calibration curves of DFS predicted by $M_{US+CEUS+clinical}$ in the different groups. DFS at (A) 24, (B) 36, and (C) 60 months for $M_{US+CEUS+clinical}$ in the training group. DFS at (D) 24, (E) 36, and (F) 60 months for $M_{US+CEUS+clinical}$ in the internal validation group. DFS at (G) 24, (H) 36, (I) and 60 months for $M_{US+CEUS+clinical}$ in the external validation group. The dashed line represents an excellent match between nomogram predictions (X-axis) and actual survival results (Y-axis). The cohort was divided into three groups with equal sample sizes for internal verification. The closer the distance from the dot to the dotted line, the higher the prediction accuracy. $M_{US+CEUS+clinical}$, nomogram model based on US, CEUS, and clinical characteristics; DFS, disease-free survival; CEUS, contrast-enhanced ultrasound; US, ultrasound.

nomogram outperformed clinicopathological models and the TNM staging system in predicting DFS for triple-negative breast cancer (P<0.01, C-indices: 0.811, 0.816, 0.816). Xiong *et al.* (32) reported superior performance of a US-based radiomics model over a clinicopathological nomogram (C-index: 0.796 *vs.* 0.761, P=0.04). However, these studies did not assess blood flow, limiting their usefulness to breast cancer prognosis prediction.

In our study, the C-indices for the $M_{US+clinical}$ model, which combined US and clinical features, were 0.794, 0.799, and 0.743 in the training, internal validation, and external validation sets, respectively. These values were higher than those for the $M_{clinical}$ model, which used only clinical features (0.788, 0.786, and 0.719, respectively). However, in the NRI and IDI analyses at 24, 36, and 60 months, the differences between the $M_{US+clinical}$ and $M_{clinical}$ nomograms were not statistically significant (P>0.05).

Although CT offers high sensitivity and specificity, it lacks established morphological criteria for evaluating postoperative DFS in patients with breast cancer (33). The application of breast MRI in determining DFS is still being explored. A retrospective analysis of 1,214 patients diagnosed with invasive breast cancer indicated that radiomics features obtained from MRI were predictive of 3-year DFS in both the development and validation cohorts, yielding an AUC of 0.81 and 0.73, respectively (34).

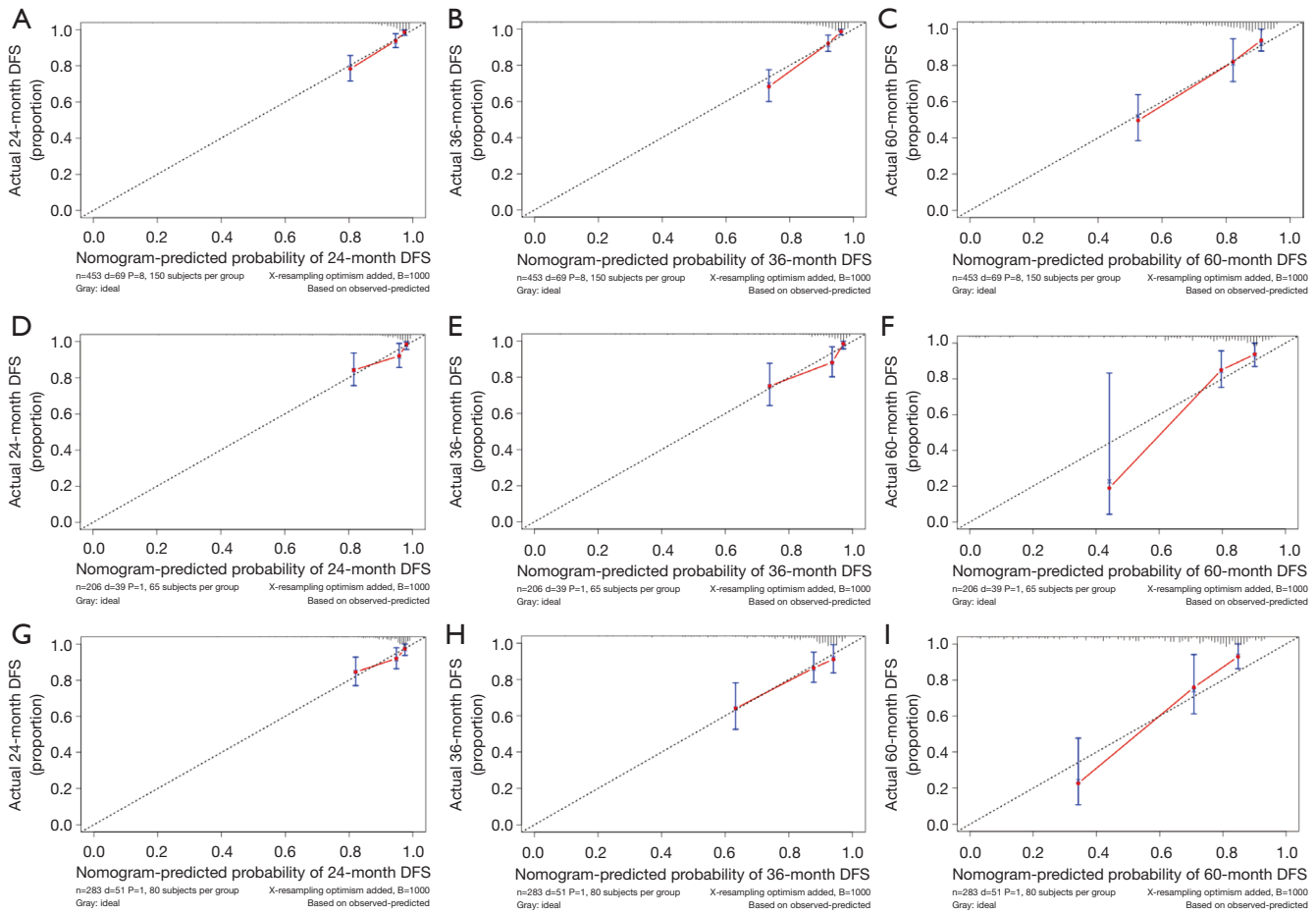

Figure 8 Calibration curves of DFS predicted by $M_{US+clinical}$ in the different groups. DFS at (A) 24, (B) 36, and (C) 60 months for $M_{US+clinical}$ in the training group. DFS at (D) 24, (E) 36, and (F) 60 months for $M_{US+clinical}$ in the internal validation group. DFS at (G) 24, (H) 36, (I) and 60 months for $M_{US+clinical}$ in the external validation group. The dashed line represents an excellent match between nomogram predictions (X-axis) and actual survival results (Y-axis). The cohort was divided into three groups with equal sample sizes for internal verification. The closer the distance from the dot to the dotted line is, the higher the prediction accuracy. $M_{US+clinical}$, nomogram model based on US and clinical characteristics; DFS, disease-free survival; US, ultrasound.

Furthermore, a clinical radiomics nomogram based on a random Forest-Cox regression model was found to be able to successfully distinguish between high-risk and low-risk patients in a development cohort [hazard ratio (HR) 0.04, 95% CI: 0.004–0.32; P<0.001] and a validation cohort with the addition of clinical variables (HR 0.04; 95% CI: 0.004–0.32; P<0.001) (34). However, the median follow-up period for patients in that study was only 23.8 months (IQR, 15.3–37.6 months), and longer follow-up period is needed in future prospective trials for validation of these results.

Breast cancer DFS has also been assessed using mammography and positron emission tomography/CT (PET/CT). A study by Luo *et al.* (35) found that mammographic radiomics features were associated with invasive DFS in breast cancer, possibly through pathways involved in cell cycle regulation. Additionally, a comprehensive model using radiomics and depth data from PET/CT images demonstrated the ability to correctly predict the 5-year DFS in patients with nonpathological complete response, yielding AUC values of 0.943 in the training cohort and 0.938 in the validation cohort (36). However, PET/CT is too costly and radiation-intensive for long-term breast cancer follow-up.

CEUS, using microbubble contrast agents with diameters of approximately 2.5 μm, offers enhanced detection of tumor in microvessels. In this study, the C-indices for

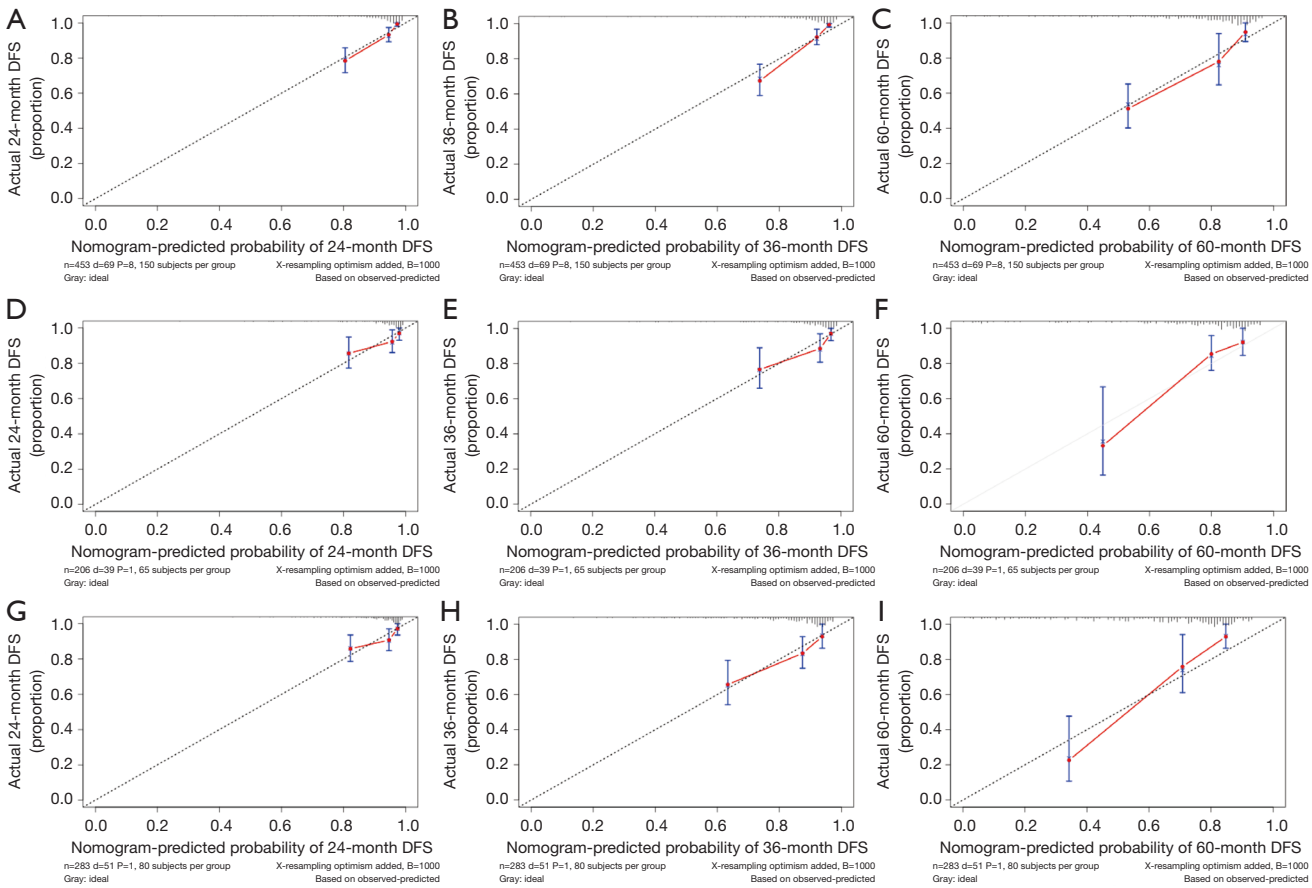

Figure 9 Calibration curves of DFS predicted by $M_{clinical}$ in the different groups. DFS at (A) 24, (B) 36, and (C) 60 months for $M_{clinical}$ in the training group. DFS at (D) 24, (E), 36, and (F) 60 months for $M_{clinical}$ in the internal validation group. DFS at (G) 24, (H) 36, and (I) 60 months for $M_{clinical}$ in the external validation group. The dashed line represents an excellent match between nomogram predictions (X-axis) and actual survival results (Y-axis). The cohort was divided into three groups with equal sample sizes for internal verification. The closer the distance from the dot to the dotted line is, the higher the prediction accuracy. $M_{clinical}$, nomogram model based on clinical characteristics. DFS, disease-free survival.

Table 7 NRI and IDI for $M_{US+CEUS+clinical}$ *vs.* $M_{US+clinical}$ in DFS prediction

Variable	Training group			Internal validation group			External validation group		
	Estimate	95% CI	P value	Estimate	95% CI	P value	Estimate	95% CI	P value
NRI (*vs.* $M_{US+clinical}$)									
For 24-month DFS	0.259	0.045, 0.364	0.02	0.376	0.012, 0.532	0.04	0.481	0.072, 0.581	0.02
For 36-month DFS	0.264	0.020, 0.468	0.04	0.308	0.022, 0.485	0.04	0.545	0.077, 0.659	0.03
For 60-month DFS	0.313	0.013, 0.488	0.04	0.378	–0.258, 0.661	0.23	0.545	–0.194, 0.943	0.10
IDI (*vs.* $M_{US+clinical}$)									
For 24-month DFS	0.036	0.006, 0.077	0.01	0.043	0.001, 0.106	0.04	0.040	0.005, 0.098	0.02
For 36-month DFS	0.051	0.003, 0.116	0.04	0.083	0.003, 0.119	0.04	0.069	0.000, 0.158	0.05
For 60-month DFS	0.055	0.007, 0.118	0.03	0.044	–0.041, 0.134	0.21	0.045	–0.150, 0.332	0.31

$M_{US+CEUS+clinical}$, nomogram model based on US, CEUS, and clinical characteristics; $M_{US+clinical}$, nomogram model based on US and clinical characteristics; NRI, net reclassification index; IDI, integrated discrimination improvement; CI, confidence interval; DFS, disease-free survival; US, ultrasound; CEUS, contrast-enhanced ultrasound.

Table 8 NRI and IDI for $M_{US+CEUS+clinical}$ *vs.* $M_{clinical}$ in DFS prediction

Variable	Training group			Internal validation group			External validation group		
	Estimate	95% CI	P value	Estimate	95% CI	P value	Estimate	95% CI	P value
NRI (*vs.* $M_{clinical}$)									
For 24-month DFS	0.202	0.073, 0.394	0.01	0.351	0.038, 0.543	0.03	0.516	0.245, 0.650	0.01
For 36-month DFS	0.253	0.030, 0.320	0.046	0.243	0.041, 0.460	0.04	0.592	0.153, 0.676	0.008
For 60-month DFS	0.267	0.034, 0.485	0.02	0.424	–0.001, 0.701	0.09	0.545	–0.260, 1.061	0.14
IDI (*vs.* $M_{clinical}$)									
For 24-month DFS	0.044	0.009, 0.093	0.01	0.051	0.000, 0.146	0.046	0.108	0.021, 0.181	<0.001
For 36-month DFS	0.031	0.001, 0.078	0.03	0.046	0.003, 0.129	0.04	0.090	0.022, 0.159	0.01
For 60-month DFS	0.067	0.015, 0.138	0.02	0.105	–0.004, 0.241	0.06	0.043	–0.226, 0.280	0.34

$M_{US+CEUS+clinical}$, nomogram model based on US, CEUS, and clinical characteristics; $M_{clinical}$, nomogram model based on clinical characteristics; NRI, net reclassification index; IDI, integrated discrimination improvement; CI, confidence interval; DFS, disease-free survival; US, ultrasound; CEUS, contrast-enhanced ultrasound.

Table 9 NRI and IDI for $M_{US+clinical}$ *vs.* $M_{clinical}$ in DFS prediction

Variable	Training group			Internal validation group			External validation group		
	Estimate	95% CI	P value	Estimate	95% CI	P value	Estimate	95% CI	P value
NRI (*vs.* $M_{US+clinical}$)									
For 24-month DFS	0.111	–0.198, 0.256	0.37	0.006	–0.206, 0.335	0.63	0.481	0.072, 0.581	0.02
For 36-month DFS	0.108	–0.206, 0.239	0.39	–0.012	1-/192, 0.280	1.32	0.545	0.077, 0.659	0.03
For 60-month DFS	0.053	–0.276, 0.284	0.72	0.427	–0.152, 0.706	0.12	0.545	–0.194, 0.943	0.10
IDI (*vs.* $M_{US+clinical}$)									
For 24-month DFS	0.008	–0.006, 0.077	0.20	0.007	–0.032, 0.083	0.71	0.040	0.005, 0.098	0.02
For 36-month DFS	0.009	–0.004, 0.038	0.21	–0.006	–0.035, 0.056	0.87	0.069	0.000, 0.158	0.05
For 60-month DFS	0.013	–0.006, 0.050	0.26	0.061	–0.002, 0.168	0.06	0.045	–0.150, 0.332	0.31

$M_{US+clinical}$, nomogram model based on US and clinical characteristics; $M_{clinical}$, nomogram model based on clinical characteristics; NRI, net reclassification index; IDI, integrated discrimination improvement; DFS, disease-free survival; US, ultrasound.

the predictive model combining US, CEUS, and clinical features was 0.811, 0.816, and 0.819 in the training, internal validation, and external validation sets, respectively; these values were higher than those for the $M_{US+clinical}$ (0.794, 0.799, and 0.743, respectively) and $M_{clinical}$ models (0.788, 0.786, and 0.719, respectively). Furthermore, in the NRI and IDI analyses, the $M_{US+CEUS+clinical}$ model outperformed the other nomograms at 24 and 36 months in all sets and at 60 months in the training set. Despite the promising results, the relatively recent adoption of CEUS presents challenges in the collection of long-term follow-up data from patients, particularly with respect to DFS.

The potential integration of emerging liquid biopsy approaches (37), such as circulating tumor cells (CTCs) and circulating tumor DNA (ctDNA), into the nomogram that combines US, CEUS, and clinical characteristics is likely to further enhance the nomogram's performance in identifying patients at an elevated risk of recurrence and metastasis.

The study involved several notable limitations. First, the operator-dependent nature of US and CEUS may introduce variability in image acquisition and interpretation. Second, its retrospective design limited the ability to conduct a quantitative CEUS analysis. Third, overall survival was not assessed, and the 5-year DFS in the validation cohort was

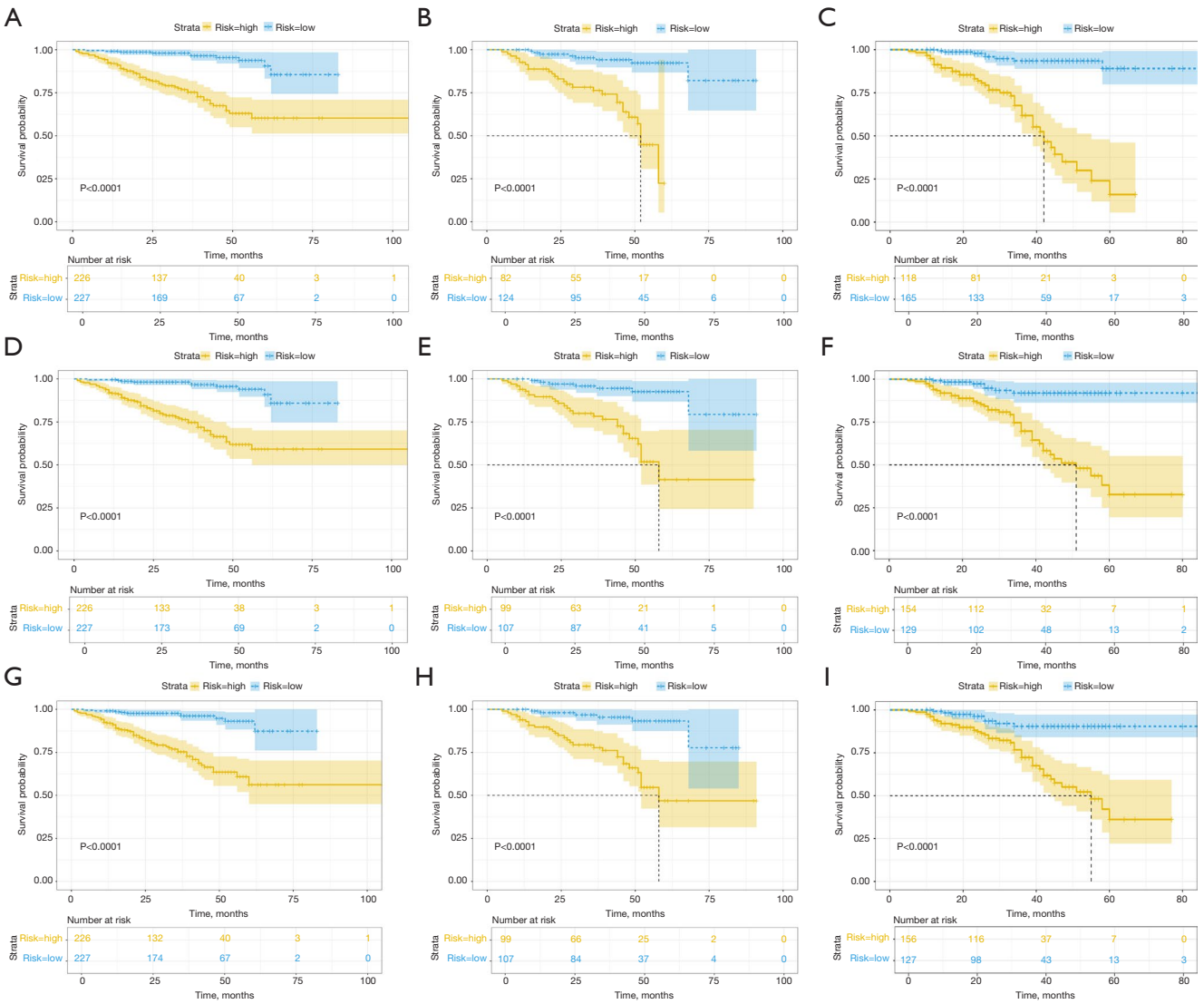

Figure 10 Kaplan-Meier survival curves for two disease-free survival subgroups of the three models. $M_{US+CEUS+clinical}$: (A) training, (B) internal validation, and (C) external validation. $M_{US+clinical}$: (D) training, (E) internal validation, and (F) external validation. $M_{clinical}$: (G) training, (H) internal validation, and (I) external validation. $M_{US+CEUS+clinical}$, nomogram model based on US, CEUS, and clinical characteristics; $M_{US+clinical}$, nomogram model based on US and clinical characteristics; $M_{clinical}$, nomogram model based on clinical characteristics; CEUS, contrast-enhanced ultrasound; US, ultrasound.

suboptimal. Future studies with longer follow-up periods and prospective validation are needed to evaluate the impact of US and CEUS imaging features on survival outcomes.

Conclusions

The nomogram combining US, CEUS, and clinical characteristics established in this study could accurately identify high-risk individuals who require more vigilant monitoring following surgery for invasive breast cancer.

Acknowledgments

None.

Footnote

Reporting Checklist: The authors have completed the

TRIPOD reporting checklist. Available at https://tcr.amegroups.com/article/view/10.21037/tcr-2025-96/rc

Data Sharing Statement: Available at https://tcr.amegroups.com/article/view/10.21037/tcr-2025-96/dss

Peer Review File: Available at https://tcr.amegroups.com/article/view/10.21037/tcr-2025-96/prf

Funding: This research was funded by the National Key R&D Program of China (No. 2023YFC2414203) and National Natural Science Foundation (No. 82371972).

Conflicts of Interest: All authors have completed the ICMJE uniform disclosure form (available at https://tcr.amegroups.com/article/view/10.21037/tcr-2025-96/coif). The authors have no conflicts of interest to declare.

Ethical Statement: The authors are accountable for all aspects of the work in ensuring that questions related to the accuracy or integrity of any part of the work are appropriately investigated and resolved. The study was conducted in accordance with the Declaration of Helsinki (as revised in 2013). This retrospective study received approval from the medical ethics committee of PLA General Hospital, China (No. S2024-749-01). All participating hospitals were informed and agreed with this study. The requirement for individual consent was waived due to the retrospective nature of the analysis.

References

1. Gradishar WJ, Moran MS, Abraham J, et al. Breast Cancer, Version 3.2024, NCCN Clinical Practice Guidelines in Oncology. J Natl Compr Canc Netw 2024;22:331-57.
2. Cardoso MJ, Poortmans P, Senkus E, et al. Breast cancer highlights from 2023: Knowledge to guide practice and future research. Breast 2024;74:103674.
3. Zhong YM, Tong F, Shen J. Lympho-vascular invasion impacts the prognosis in breast-conserving surgery: a systematic review and meta-analysis. BMC Cancer 2022;22:102.
4. Boughey JC, Rosenkranz KM, Ballman KV, et al. Local Recurrence After Breast-Conserving Therapy in Patients With Multiple Ipsilateral Breast Cancer: Results From ACOSOG Z11102 (Alliance). J Clin Oncol 2023;41:3184-93.
5. Kunkler IH, Williams LJ, Jack WJL, et al. Breast-Conserving Surgery with or without Irradiation in Early Breast Cancer. N Engl J Med 2023;388:585-94.
6. Lynch JA, Berse B, Coomer N, et al. 21-Gene recurrence score testing among Medicare beneficiaries with breast cancer in 2010-2013. Genet Med 2017;19:1134-43.
7. Kalinsky K, Barlow WE, Gralow JR, et al. 21-Gene Assay to Inform Chemotherapy Benefit in Node-Positive Breast Cancer. N Engl J Med 2021;385:2336-47.
8. Cannioto RA, Hutson A, Dighe S, et al. Physical Activity Before, During, and After Chemotherapy for High-Risk Breast Cancer: Relationships With Survival. J Natl Cancer Inst 2021;113:54-63.
9. Qu FL, Wu SY, Li JJ, et al. Ipsilateral breast tumor recurrence after breast-conserving surgery: insights into biology and treatment. Breast Cancer Res Treat 2023;202:215-20.
10. Pan H, Gray R, Braybrooke J, et al. 20-Year Risks of Breast-Cancer Recurrence after Stopping Endocrine Therapy at 5 Years. N Engl J Med 2017;377:1836-46.
11. Guo S, Guo L, Li J, et al. Construction of a prognostic survival model with tumor immune-related genes for breast cancer. Transl Cancer Res 2024;13:6919-35.
12. Ma J, Wu Z, Xu Y, et al. Survival outcomes, multidimensional prediction and subsequent therapy in patients with hormone receptor-positive advanced breast cancer receiving palbociclib: a real-world analysis. Gland Surg 2024;13:2313-24.
13. Liu H, Bao H, Zhao J, et al. Establishment and verification of a prognostic immune cell signature-based model for breast cancer overall survival. Transl Cancer Res 2024;13:5600-15.
14. Candido Dos Reis FJ, Wishart GC, Dicks EM, et al. An updated PREDICT breast cancer prognostication and treatment benefit prediction model with independent validation. Breast Cancer Res 2017;19:58.
15. Pan B, Xu Y, Yao R, et al. Nomogram prediction of the 70-gene signature (MammaPrint) binary and quartile categorized risk using medical history, imaging features

and clinicopathological data among Chinese breast cancer patients. J Transl Med 2023;21:798.
16. Park H, Lim Y, Ko ES, et al. Radiomics Signature on Magnetic Resonance Imaging: Association with Disease-Free Survival in Patients with Invasive Breast Cancer. Clin Cancer Res 2018;24:4705-14.
17. Boca Bene I, Dudea SM, Ciurea AI. Contrast-Enhanced Ultrasonography in the Diagnosis and Treatment Modulation of Breast Cancer. J Pers Med 2021;11:81.
18. Collins GS, Reitsma JB, Altman DG, et al. Transparent reporting of a multivariable prediction model for individual prognosis or diagnosis (TRIPOD): the TRIPOD statement. BMJ 2015;350:g7594.
19. American Joint Committee on Cancer. AJCC cancer staging manual (9th ed.). Springer; 2019.
20. Li JK, Fu NQ, Wang B, et al. Conventional ultrasound combined with contrast-enhanced ultrasound: could it be helpful for the diagnosis of thoracic wall recurrence after mastectomy? Eur Radiol 2023;33:6482-91.
21. Phung MT, Tin Tin S, Elwood JM. Prognostic models for breast cancer: a systematic review. BMC Cancer 2019;19:230.
22. Wang S, Xiong Y, Zhang Q, et al. Clinical significance and immunogenomic landscape analyses of the immune cell signature based prognostic model for patients with breast cancer. Brief Bioinform 2021;22:bbaa311.
23. Hueting TA, van Maaren MC, Hendriks MP, et al. External validation of 87 clinical prediction models supporting clinical decisions for breast cancer patients. Breast 2023;69:382-91.
24. Zuo D, Yang L, Jin Y, et al. Machine learning-based models for the prediction of breast cancer recurrence risk. BMC Med Inform Decis Mak 2023;23:276.
25. Seibel AJ, Kelly OM, Dance YW, et al. Role of Lymphatic Endothelium in Vascular Escape of Engineered Human Breast Microtumors. Cell Mol Bioeng 2022;15:553-69.
26. Zeng H, Hou Y, Zhou X, et al. Cancer-associated fibroblasts facilitate premetastatic niche formation through lncRNA SNHG5-mediated angiogenesis and vascular permeability in breast cancer. Theranostics 2022;12:7351-70.
27. de Heer EC, Jalving M, Harris AL. HIFs, angiogenesis, and metabolism: elusive enemies in breast cancer. J Clin Invest 2020;130:5074-87.
28. Liu X, Wang M, Wang Q, et al. Diagnostic value of contrast-enhanced ultrasound for sentinel lymph node metastasis in breast cancer: an updated meta-analysis. Breast Cancer Res Treat 2023;202:221-31.
29. Coffey K, Jochelson MS. Contrast-enhanced mammography in breast cancer screening. Eur J Radiol 2022;156:110513.
30. Wang K, Chen Q, Liu N, et al. Recent advances in, and challenges of, anti-angiogenesis agents for tumor chemotherapy based on vascular normalization. Drug Discov Today 2021;26:2743-53.
31. Yu F, Hang J, Deng J, et al. Radiomics features on ultrasound imaging for the prediction of disease-free survival in triple negative breast cancer: a multi-institutional study. Br J Radiol 2021;94:20210188.
32. Xiong L, Chen H, Tang X, et al. Ultrasound-Based Radiomics Analysis for Predicting Disease-Free Survival of Invasive Breast Cancer. Front Oncol 2021;11:621993.
33. Zhu Y, O'Connell AM, Ma Y, et al. Dedicated breast CT: state of the art-Part II. Clinical application and future outlook. Eur Radiol 2022;32:2286-300.
34. Yu Y, Tan Y, Xie C, et al. Development and Validation of a Preoperative Magnetic Resonance Imaging Radiomics-Based Signature to Predict Axillary Lymph Node Metastasis and Disease-Free Survival in Patients With Early-Stage Breast Cancer. JAMA Netw Open 2020;3:e2028086.
35. Luo C, Zhao S, Peng C, et al. Mammography radiomics features at diagnosis and progression-free survival among patients with breast cancer. Br J Cancer 2022;127:1886-92.
36. Zheng X, Huang Y, Lin Y, et al. (18)F-FDG PET/CT-based deep learning radiomics predicts 5-years disease-free survival after failure to achieve pathologic complete response to neoadjuvant chemotherapy in breast cancer. EJNMMI Res 2023;13:105.
37. Stergiopoulou D, Markou A, Strati A, et al. Comprehensive liquid biopsy analysis as a tool for the early detection of minimal residual disease in breast cancer. Sci Rep 2023;13:1258.

(English Language Editor: J. Gray)

Cite this article as: Li S, Li Y, Fang Y, Jin Z, Huang S, Wang W, Mokbel K, Xu Y, Yang H, Wang Z. Enhancing prognostic accuracy in invasive breast cancer by combining contrast-enhanced ultrasound and clinical data: a multicenter retrospective study. Transl Cancer Res 2025;14(2):1336-1358. doi: 10.21037/tcr-2025-96

